Contributions to Geophysics and Geodesy Vol. 53/4, 2023 (319–331)

On the practical implementation of the enhanced horizontal derivative filter for potential field data

Saulo Pomponet OLIVEIRA[1,2,*], Alessandra de Barros e Silva BONGIOLO[2,3], Luan Thanh PHAM[4], Luís Gustavo DE CASTRO[2,3], Vinicius Theobaldo JORGE[2]

[1] Federal University of Paraná, Department of Mathematics, Curitiba, Brazil
[2] Federal University of Paraná, Graduate Program in Geology, Curitiba, Brazil
[3] Federal University of Paraná, Department of Geology, Curitiba, Brazil
[4] University of Science, Vietnam National University, Hanoi, Vietnam

Abstract: The enhanced horizontal derivative (EHD) is an enhancement filter whose maxima provide estimated locations of the sources' boundaries. This filter is defined as the total horizontal derivative (THDR) of a weighted sum of vertical derivatives of increasing order. We consider some aspects of the practical implementation of the EHD filter, especially its robustness. A slightly different version of EHD, which we refer to as mEHD, is obtained when we switch the order of THDR and the weighted sum; that is, when we consider the weighted sum of total horizontal derivatives of the successive vertical derivatives. It turns out that mEHD can be more stable and provide a clearer enhanced map than the original filter, as demonstrated with examples of synthetic data and aeromagnetic data from Southern Brazil. Moreover, we address the choice of the weighting coefficients of the vertical derivatives, emphasizing that the standard choice of unitary weights may not be the most appropriate one.

Key words: gravimetry, magnetometry, enhanced horizontal derivative

1. Introduction

The enhanced horizontal derivative (EHD) proposed by *Fedi and Florio (2001)* is a derivative filter for potential field data that increases the resolution of the total horizontal derivative (THDR, *Cordell and Grauch, 1985*). Rather than computing the THDR of the anomalous field, EHD considers a transformed field that resembles the Taylor-series expansion of downward continued data, but it has a simpler expression and gives more importance to the high-order derivative terms. EHD has become a popular tool for

*corresponding author, e-mail: saulopo@ufpr.br

doi: 10.31577/congeo.2023.53.4.1

delineating lateral boundaries and depth estimation (e.g., *Debeglia et al., 2005; Louro et al., 2014*). Moreover, EHD serves as a tool for multiscale analysis (*Fedi, 2002; Cella and Fedi, 2015*).

Despite its simple formulation, this method requires caution with some aspects of its implementation to attain reliable results (*Fedi and Florio, 2001*). Similarly to THDR, magnetic data should be reduced to the pole or transformed into a pseudogravity map so that the maxima of EHD are more likely to be positioned over the sources' edges. Moreover, high-order vertical derivatives should not be computed with the standard approach in the Fourier domain, otherwise noise will be significantly amplified. One can use the integrated second vertical derivative (ISVD, *Fedi and Florio, 2001*) or some other strategy to compute stable vertical derivatives (e.g., *Richter and Pašteka, 2003; Pašteka et al., 2009; Oliveira and Pham, 2022*). Finally, EHD was designed under the assumption of a unitary grid cell. For field data with non-unitary grid spacing, the contribution of higher-order derivatives may be compromised.

Our contribution focuses on the latter two implementation aspects. For the development of the multiscale derivative analysis method, *Fedi (2002)* considered a slightly different version of EHD, which we refer to as mEHD. We observed from numerical experiments that mEHD is less sensitive to noise than EHD, although the difference between them is negligible in some cases. We also review the choices of the weighting factors of the transformed anomaly that defines EHD. We illustrate through synthetic and field examples that these factors should depend on the grid spacing.

2. Theory

Let us first review the derivation of the enhanced horizontal derivative filter. Its starting point is the Taylor-series expansion of downward-continued field data:

$$f(x_j, y_j, z_0 + h_c) = f(x_j, y_j, z_0) + h_c f^{(1)}(x_j, y_j, z_0) + \frac{h_c^2}{2!} f^{(2)}(x_j, y_j, z_0) + \cdots + \frac{h_c^m}{m!} f^{(m)}(x_j, y_j, z_0), \quad (1)$$

where $f^{(i)}(x_j, y_j, z_0)$ denotes the discrete i-th vertical derivative of the potential data f at the observation plane $z = z_0$ and the j-th grid point

(x_j, y_j), while h_c is the continuation height. This parameter is typically chosen as being equal to or proportional to the grid spacing Δs (*Fedi and Florio, 2001; Tran and Nguyen, 2020*). In the simpler case where $h_c = 1$,

$$f(x_j, y_j, z_0 + 1) = f(x_j, y_j, z_0) + f^{(1)}(x_j, y_j, z_0) + \cdots + \frac{1}{m!} f^{(m)}(x_j, y_j, z_0). \quad (2)$$

For conciseness, we omit the dependence of f on z from here on. *Fedi and Florio (2001)* proposed the general transformed field:

$$\phi(x_j, y_j) = w_0 f(x_j, y_j) + w_1 f^{(1)}(x_j, y_j) + \cdots + w_m f^{(m)}(x_j, y_j), \quad (3)$$

and then defined EHD = THDR(ϕ), where THDR($\cdot$) denotes the total horizontal derivative, i.e, the magnitude of the horizontal gradient:

$$\mathrm{THDR}(g) = \sqrt{\left(\frac{\partial g}{\partial x}\right)^2 + \left(\frac{\partial g}{\partial y}\right)^2} = \|\nabla_h g\|, \quad \nabla_h g = \left(\frac{\partial g}{\partial x}, \frac{\partial g}{\partial y}\right). \quad (4)$$

Arguing that the factorial weights in equation (1) reduce the importance of the higher-order terms, *Fedi and Florio (2001)* suggested the simple choice $w_0 = \ldots = w_m = 1$, which is the most widely used in the literature. However, this choice may not be appropriate if $h_c \gg 1$ as the coefficients of the higher-order terms would be severely reduced. Likewise, these terms would be overemphasized if $h_c \ll 1$, which may cause numerical instability. Thus, a more suitable choice would be $w_i = h_c^i$. *Fedi (2002)* proposed the more general choice $w_i = k^i$ for some constant k chosen by the user. In this sense, the EHD with unitary weights and with Fedi's choice can be seen as an approximate downward continuation with heights $h_c = 1$ and $h_c = k$, respectively. To guarantee that all terms in equation (3) have the same units, we can choose the constant k to be proportional to the grid spacing Δs. In this case, ϕ has the same unit as the anomalous field.

We assume $w_i > 0$ $(0 \leq i \leq m)$ from here on. Rather than defining EHD = THDR($w_0 f + w_1 f^{(1)} + \ldots + w_m f^{(m)}$), one may also consider a modified form which is also mentioned by *Fedi (2002)*:

$$\mathrm{mEHD} = w_0 \mathrm{THDR}(f) + w_1 \mathrm{THDR}(f^{(1)}) + \ldots + w_m \mathrm{THDR}(f^{(m)}). \quad (5)$$

We remark that EHD and mEHD are not equivalent in general. Indeed, by successively using the triangle inequality $\|\vec{x} + \vec{y}\| \leq \|\vec{x}\| + \|\vec{y}\|$, we find:

$$\left\| \sum_{i=0}^{m} \vec{x}_i \right\| \leq \sum_{i=0}^{m} \|\vec{x}_i\|. \tag{6}$$

Choosing $\vec{x}_i = w_i \nabla_h f^{(i)}$ $(0 \leq i \leq m)$ in equation (6) yields:

$$\text{EHD} \leq \text{mEHD}. \tag{7}$$

3. Examples

In the following, the relationship between EHD and mEHD is further explored in the enhancement of synthetic and real magnetic data. For conciseness, we employ $m = 6$ in most examples. The weights are $w_i = \Delta s^i$, unless stated otherwise.

3.1. Vertical step

Let us begin with the theoretical example of a 2D step model with depth to the top h, where we can clearly see the differences between mEHD and EHD, considering the simple case of unitary weights.

Following *Nabighian (1972)*, the horizontal and vertical derivatives of the magnetic anomaly $f = f(x, z)$, when the effective dip angle ϕ is zero, are:

$$\frac{\partial f}{\partial x} = A \frac{h - z}{x^2 + (h - z)^2}, \quad \frac{\partial f}{\partial z} = A \frac{x}{x^2 + (h - z)^2}, \tag{8}$$

where A is an amplitude factor that does not depend on x or z. From these expressions we can find explicit formulas for EHD and mEHD of order $m = 1$ evaluated at $z = 0$:

$$\text{EHD} = \sqrt{\left(\frac{\partial f}{\partial x} + \frac{\partial^2 f}{\partial z \partial x} \right)^2} = |A| \frac{\left| h^2 - x^2 + h(h^2 + x^2) \right|}{(x^2 + h^2)^2}, \tag{9}$$

$$\text{mEHD} = \sqrt{\left(\frac{\partial f}{\partial x} \right)^2} + \sqrt{\left(\frac{\partial^2 f}{\partial z \partial x} \right)^2} = |A| \frac{\left| h^2 - x^2 \right| + h \left| h^2 + x^2 \right|}{(x^2 + h^2)^2}. \tag{10}$$

Note that EHD = mEHD if $|x| \leq h$. Otherwise, $h^2 - x^2 < 0$, and thus EHD < mEHD. In general, as shown in Fig. 1, EHD and mEHD are identical in the neighborhood of the step discontinuity.

3.2. Two prismatic sources

In analogy with the example from *Fedi (2002)*, we consider a model of two

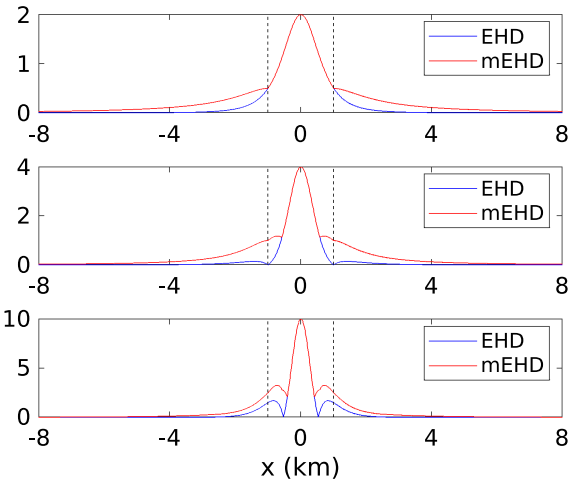

Fig. 1. EHD and mEHD of a vertical step with depth $h = 1$ km, normalized by the absolute value of the amplitude, $|A|$. From top to bottom: $m = 1$, $m = 2$, and $m = 3$.

interfering prismatic sources with square cross-section, whose parameters are presented in Table 1. Figure 2a shows the total field anomaly generated according to *Rao and Babu (1991)*, with declination $D = 0°$, inclination $I = 90°$, and $\Delta s = 1$ km. We also added Gaussian random noise with standard deviation corresponding to 1% of the maximum absolute value of the anomaly (Fig. 2d).

Table 1. Parameters of the magnetic model of two prismatic sources.

Parameter	P1	P2
Easting coordinates of center (km)	120	90
Northing coordinates of center (km)	120	90
Width (km)	50	60
Length (km)	50	60
Depth of top (km)	7	9
Depth of bottom (km)	9	13
Magnetization (A/m)	1.5	2

Let us compare mEHD with EHD, considering the approximation order $m = 6$. Figures 2b and 2c show the EHD and mEHD maps of the noise-free data, which are very similar. Figures 2e and 2f correspond to the same maps

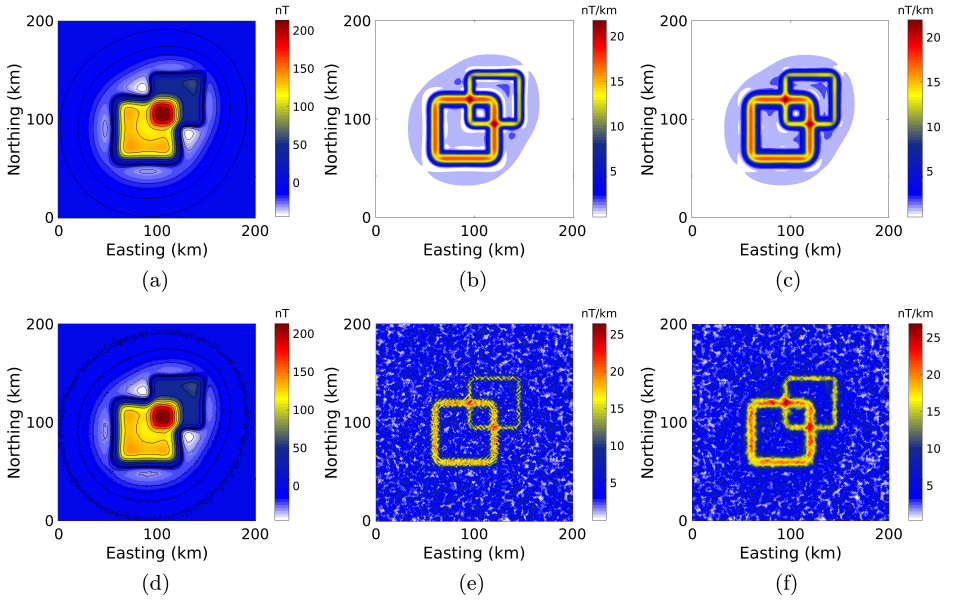

Fig. 2. Total field anomaly (a) of the model described by Table 1; EHD (b) and mEHD (c) of the data in (a); (d) data in (a) corrupted with Gaussian random noise with standard deviation corresponding to 1% of the maximum absolute value of the anomaly; EHD (e) and mEHD (f) of the data in (d).

for the noise-corrupted data. Although both maps are severely affected by noise, mEHD delineates the sources' edges in a more continuous manner, and the smaller prism is more visible than in the EHD map.

Vertical profiles were extracted from the EHD and mEHD maps and are shown in Fig. 3. In the noise-free case (Fig. 3a), the differences between these maps are more clearly visible in the profile. In the noisy case (Fig. 3b), we can note that mEHD provides better approximations over the

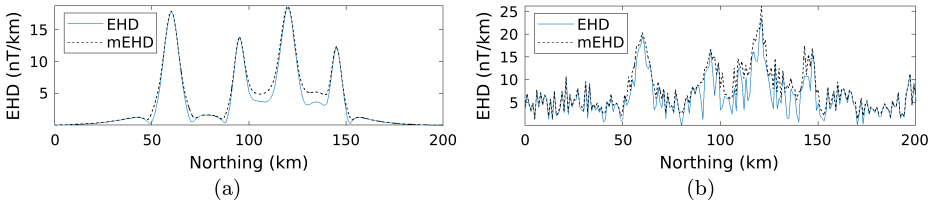

Fig. 3. Profiles of the EHD and mEHD maps from Fig. 2 at $x = 100$ km: (a) noise-free data; (b) noise-corrupted data.

true anomalies, while it nearly coincides with EHD away from them. On both profiles, mEHD can be described as an envelope of EHD.

Figure 4 illustrates the relevance of choosing the weighting factors w_i according to the grid spacing Δs. We consider the synthetic data scaled by a factor of two. Note that the profile of EHD obtained using $w_i = \Delta s^i$ ($\Delta s = 2$ km due to the scaling) is consistent with the profile in Fig. 3a, unlike the default choice $w_i = 1$.

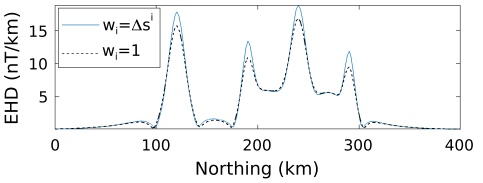

Fig. 4. Vertical profile of EHD at $x = 200$ km, considering the data from the model of prismatic sources scaled by a factor of two.

3.3. Aeromagnetic data from Vargeão Dome, Brazil

The Vargeão Dome, located on the Paraná Basin, is composed by volcanic and acid rocks from the Serra Geral Formation and brecciated rocks, probably originated from an impact event (*Kazzuo-Vieira et al., 2009*). The structures are composed of radial fractures and regional lineaments (faults) with orientations EW and ENE north of the dome and NE–SW south of the dome (Fig. 5).

Figure 6a shows the total-field anomaly acquired in 1980 by Petróleo Brasileiro S.A. (*CPRM, 1995, Project Code 4023*) with flight lines in the N–S direction, 2 km apart, and mean terrain clearance $h = 0.5$ km. The data was interpolated by the bidirectional method with grid spacing $\Delta s = 0.5$ km and reduced to the pole for an inclination $I = -26.5°$ and a declination $D = -12°$. Although the THDR map (Fig. 6b) can detect the regional lineaments, the anomalies related to the radial structures may be confounded to be part of the lineaments. On the other hand, the EHD and mEHD maps with $m = 6$ (Figs. 6c–6d) emphasize the radial structures and the interference between radial and linear fractures. As in the synthetic examples, the vertical profiles highlight that mEHD behaves as an envelope of EHD (Fig. 7).

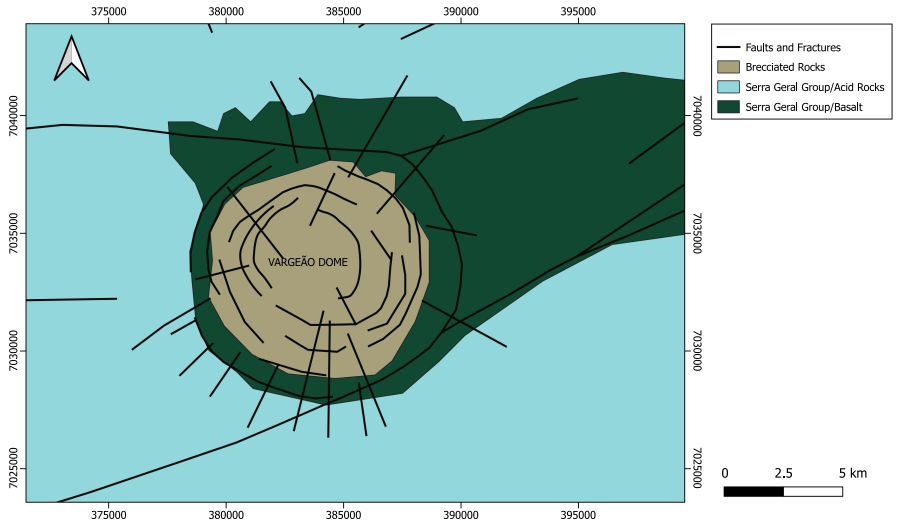

Fig. 5. Simplified geological map of the Vargeão Dome study area. Adapted from *Kazzuo-Vieira et al. (2009)*.

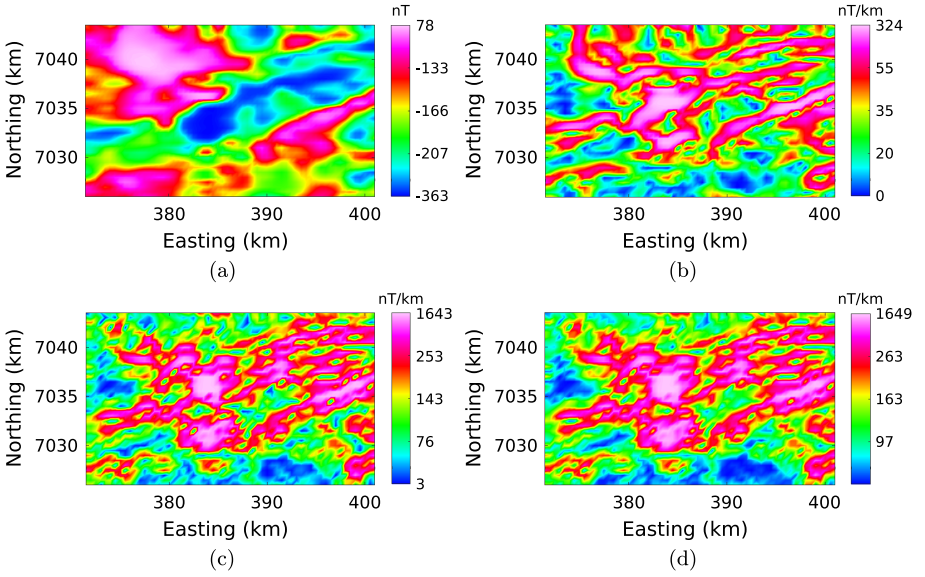

Fig. 6. (a) Reduced-to-the-pole total-field anomaly from the Vargeão Dome study area; (b) THDR of the data in (a); (c) EHD of the data in (a) with $m = 6$; (d) mEHD of the data in (a) with $m = 6$.

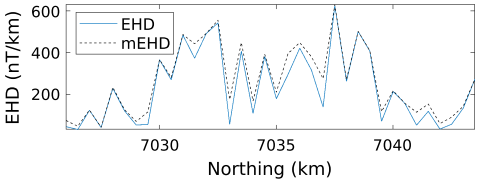

Fig. 7. Vertical profiles of the EHD and mEHD maps from Fig. 6 at $x = 385.5$ km.

3.4. Aeromagnetic data from eastern Paraná state, Brazil

Our second study area, outlined in Fig. 8, corresponds to the Meso to Neoproterozoic basement of eastern Paraná state. This area encompasses rocks from the Açungui Supergroup, Itaiacoca Group, Três Córregos and Cunhaporanga Granitic Suites, Castro Group, Paraná Basin, and alluvial deposits. The magnetic field in this area is strongly influenced by mafic dikes of Lower Cretaceous age, typically with a preferential N40–60W orientation. These dikes consist mainly of diabases, or in smaller proportions, diorites and quartz monzodiorites (*Guimarães et al., 2001*).

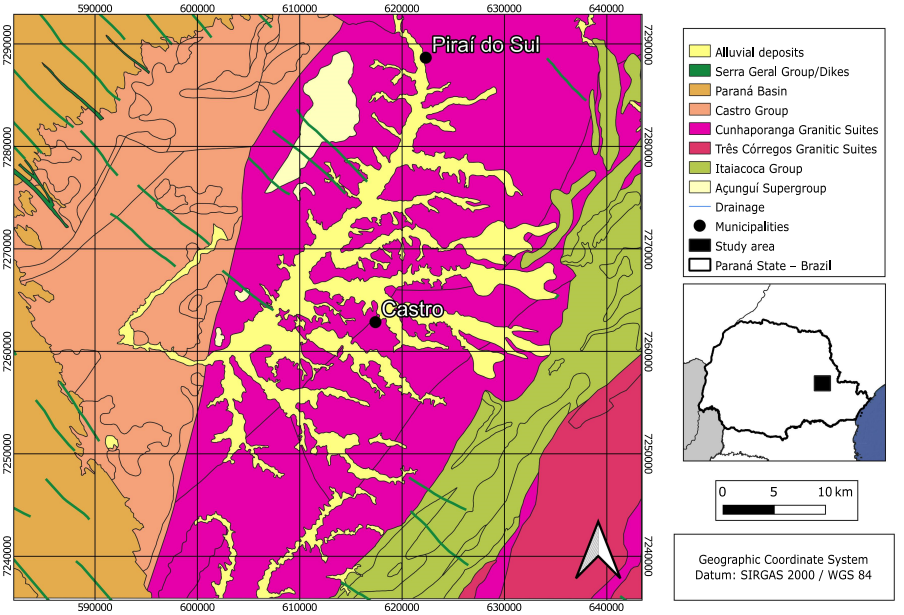

Fig. 8. Simplified geological map of the eastern Paraná study area.

We employ aeromagnetic data acquired by the Geological Survey of Brazil (*CPRM, 2011*) with flight lines in the N–S direction, 0.5 km apart, and mean terrain clearance $h = 0.1$ km. The data was interpolated by the bidirectional method with grid spacing $\Delta s = 0.1$ km and reduced to the pole considering $I = -37.61°$ and $D = -19.98°$ (Fig. 9a). The THDR map is shown in Fig. 9b, while the EHD and mEHD maps of order $m = 6$ are shown in Figs. 9c and 9d. As shown in these maps and in a vertical profile (Fig. 10a), there are no significant differences between mEHD and EHD in this example. In general, either of these approaches can be chosen by the user for high-frequency data. In this example, the enhanced derivative maps did not significantly improve the resolution with respect to the THDR map, but rather amplified the noise.

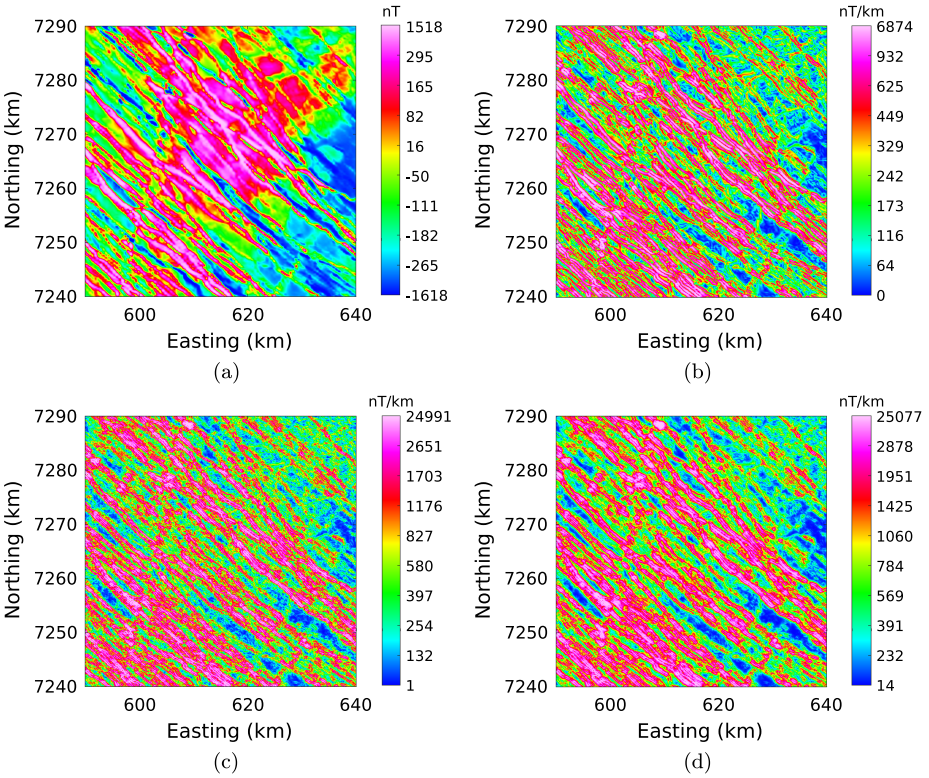

Fig. 9. Total-field anomaly (a), THDR (b), EHD (c), and mEHD (d) of the aeromagnetic data from eastern Paraná study area.

On the other hand, the values of the weights w_i are crucial to the stability of the enhanced maps. The default choice of unitary weights (Fig. 10b) is unstable, as it is related to the downward continuation of 1 km, which is ten times larger than the mean terrain clearance.

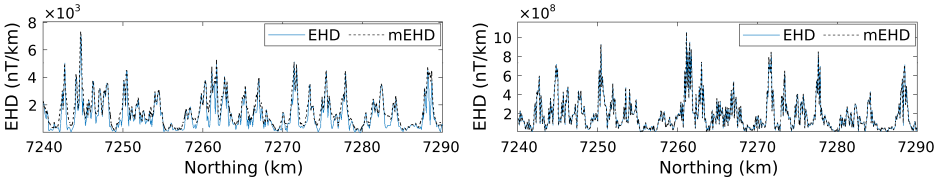

(a) (b)

Fig. 10. Vertical profiles of the EHD and mEHD maps for the data in Fig. 9a at $x = 610$ km using $w_i = \Delta s^i$ (a) and $w_i = 1$ (b).

4. Conclusions

We have outlined the potential advantages of using a modified implementation of the EHD filter, mEHD, and properly choosing its weighting factors $w_0, \ldots, w_m$. These actions may lead to more effective results with the enhanced horizontal derivative filter, improving numerical stability and the continuity of the enhanced anomalies. From the mathematical point of view, mEHD constitutes an upper bound (and also an envelope, as shown in the examples) of EHD. Qualitatively, the mEHD maps seem to show fewer high-frequency anomalies than EHD, especially in the noisy synthetic example and in the Vargeão dome study area, which can be useful for interpretation. On the other hand, the differences between EHD and mEHD may be negligible in some cases, as illustrated in the eastern Paraná study area. In those cases, a lower-order enhanced method may be preferable.

Acknowledgements. We thank the audience's feedback from a poster session at EAGE Annual 2023, where our work was presented in a preliminary version (*Oliveira et al., 2023*). We are also grateful to Rodoilton Stevanato from Laboratory for Research in Applied Geophysics (LPGA) for his help with in pre-processing the field data. S. P. Oliveira and V. T. Jorge are supported by National Council of Technological and Scientific Development (CNPq, Grant number 316376/2021-3) and Coordenação de Aperfeiçoamento de Pessoal de Nível Superior – Brasil (CAPES) – Finance Code 001, respectively. We acknowledge the support from Araucária Foundation-Brazil PI 08/2020 PIN2020141000001 as part of the Newton Fund Impact Scheme 537134315 – Supporting Sustainable Groundwater Supply Management in Brazil.

References

Cella F., Fedi M., 2015: High-resolution geophysical 3D imaging for archaeology by magnetic and EM data: the case of the Iron Age settlement of Torre Galli, Southern Italy. Surv. Geophys., **36**, 6, 831–850, doi: 10.1007/s10712-015-9341-3.

Cordell L., Grauch V. J. S., 1985: Mapping basement magnetization zones from aeromagnetic data in the San Juan Basin, New Mexico. In: Hinze W. J. (Ed.): The utility of regional gravity and magnetic anomaly maps, Society of Exploration Geophysicists, pp. 181–197, doi: 10.1190/1.0931830346.ch16.

CPRM (Geological Survey of Brazil), 1995: The Brazil Aerogeophysical Projects Database. https://www.sgb.gov.br/aero/aero.htm (accessed on November 20th 2023).

CPRM (Geological Survey of Brazil), 2011: Aerogeophysical project Paraná–Santa Catarina: survey and processing of magnetometric and gamma-ray spectrometric data. Technical report, Lasa Prospecções (in Portuguese).

Debeglia N., Martelet G., Perrin J., Truffert C., Ledru P., Tourlière B., 2005: Semi-automated structural analysis of high resolution magnetic and gamma-ray spectrometry airborne surveys. J. Appl. Geophys., **58**, 1, 13–28, doi: 10.1016/j.jappgeo.2005.03.003.

Fedi M., 2002: Multiscale derivative analysis: A new tool to enhance detection of gravity source boundaries at various scales. Geophys. Res. Lett., **29**, 2, 16-1–16-4, doi: 10.1029/2001GL013866.

Fedi M., Florio G., 2001: Detection of potential fields source boundaries by enhanced horizontal derivative method. Geophys. Prospect., **49**, 1, 40–58, doi: 10.1046/j.1365-2478.2001.00235.x.

Guimarães G. B., Ferreira F. J. F., Ulbrich H. H. G. J., Forlin M., 2001: The aerogeophysical project Serra do Mar Sul in the region of the Cunhaporanga Granitic Complex, Paraná, southern Brazil: analysis of the gamma-ray spectrometric survey. Rev. Bras. Geofis., **19**, 1, 3–18, doi: 10.1590/S0102-261X2001000100001.

Kazzuo-Vieira C., Crósta A. P., Gamboa F., Tygel M., 2009: Geophysical characterization of the Vargeão Dome impact structure, Brazil (Caracterização geofísica da estrutura de impacto do domo de Vargeão, Brasil). Rev. Bras. Geofis., **27**, 3, 375–388, doi: 10.1590/S0102-261X2009000300006 (in Portuguese with English abstract).

Louro V. H. A., Mantovani M. S. M., Ribeiro V. B., 2014: Magnetic field analysis of Morro do Leme nickel deposit. Geophysics, **79**, 6, K1–K9, doi: 10.1190/GEO2014-0131.1.

Nabighian M. N., 1972: The analytic signal of two-dimensional magnetic bodies with polygonal cross-section: its properties and use for automated anomaly interpretation. Geophysics, **37**, 3, 507–517, doi: 10.1190/1.1440276.

Oliveira S. P., Pham L. T., 2022: A stable finite difference method based on upward continuation to evaluate vertical derivatives of potential field data. Pure Appl. Geophys., **179**, 12, 4555–4566, doi: 10.1007/s00024-022-03164-z.

Oliveira S. P., Pham L. T., Bongiolo A. B. S., Jorge V. T., 2023: On the stability and effective weighting of the enhanced horizontal derivative filter. In: 84th EAGE Annual Conference & Exhibition, European Association of Geoscientists & Engineers, pp. 1–5, doi: 10.3997/2214-4609.202310237.

Pašteka R., Richter F. P., Karcol R., Brazda K., Hajach M., 2009: Regularized derivatives of potential fields and their role in semi-automated interpretation methods. Geophys. Prospect., **57**, 4, 507–516, doi: 10.1111/j.1365-2478.2008.00780.x.

Rao D. B., Babu N. R., 1991: A rapid method for three-dimensional modeling of magnetic anomalies. Geophysics, **56**, 11, 1729–1737, doi: 10.1190/1.1442985.

Richter P., Pašteka R., 2003: Influence of norms on calculation of regularized derivatives in geophysics. Contrib. Geophys. Geod., **33**, 1, 1–16.

Tran K. V., Nguyen T. N., 2020: A novel method for computing the vertical gradients of the potential field application to downward continuation. Geophys. J. Int., **220**, 2, 1316–1329, doi: 10.1093/gji/ggz524.